Applied Mechanics and Materials Vol. 828 (2016) pp 175-196
© (2016) Trans Tech Publications, Switzerland
doi:10.4028/www.scientific.net/AMM.828.175

Submitted: 2015-10-16
Accepted: 2015-10-19

High-Fidelity and Computationally Efficient Component-Wise Structural Models: an Overview of Applications and Perspectives

Marco Petrolo[a*], Erasmo Carrera[b]

Politecnico di Torino, Department of Mechanical and Aerospace Engineering,
Corso Duca degli Abruzzi 24, 10129, Torino, Italy

[a]marco.petrolo@polito.it, [b]erasmo.carrera@polito.it

* corresponding author

Keywords: CUF, Component-Wise, Dynamics, Damage.

Abstract. The Component-Wise approach (CW) is a novel structural modeling strategy that stemmed from the Carrera Unified Formulation (CUF). This work presents an overview of the enhanced capabilities of the CW for the static and dynamic analysis of structures, such as aircraft wings, civil buildings, and composite plates. The CW makes use of the advanced 1D CUF models. Such models exploit Lagrange polynomial expansions (LE) to model the displacement field above the cross-section of the structure. The use of LE allows the improvement of the 1D model capabilities. LE models provide 3D-like accuracies with far fewer computational costs. The use of LE leads to the CW. Although LE are 1D elements, every component of an engineering structure can be modeled via LE elements independently of their geometry, e.g. 2D transverse stiffeners and panels, and of their scale, e.g. fiber/matrix cells. The use of the same type of finite elements facilitates the finite element modeling to a great extent. For instance, no interface techniques are necessary. Moreover, in a CW model, the displacement unknowns are placed along the physical surfaces of the structure with no need for artificial lines and surfaces. Such a feature is promising in a CAD/FEM coupling scenario. The CW approach can be considered as an accurate and computationally cheap analysis tool for many structural problems. Such as progressive failure analyses, multiscale, impact problems and health-monitoring.

Introduction

One-dimensional (1D) structural models - or beams - are computationally cheap and efficient. The 1D modeling allows a 3D problem to be solved via a set of 1D variables, which only depend on the beam axis coordinate. 1D structural elements present many advantages that make them more efficient than 2D (plate/shell) or 3D (solid) elements. For instance, in a finite element (FE) scenario, beam models have no aspect ratio constraints. These features make beams still very appealing for the static and dynamic analyses of structures. Beam models have been developed and exploited extensively over the last few decades for the structural analysis of slender bodies, such as columns, arches, blades, aircraft wings and bridges. This work presents an overview of a novel, component-wise (CW) modeling approach based on advanced beam models that widen the application scenarios of beams to many structural problems that are usually addressable by 2D or 3D models only.
Classical beam models are those by Euler-Bernoulli [1, 2] and Timoshenko [3]. In this work, the former is referred to as EBBT, while the latter as TBT. The linear distribution of axial strain along the cross-section under bending was also correctly hypothesized by Leonardo Da Vinci [4]. These models are essentially based on a linear axial, out-of-plane displacement field and a constant transverse, in-plane displacement field. EBBT can be used for the bending of homogenous, compact, isotropic structures. TBT can be seen as an enhancement of EBBT via the addition of a uniform shear distribution above the cross-section of the beam. Since at least a parabolic distribution is required, shear correction factors are usually adopted with TBT. Such factors depend on the geometry of the cross-section. TBT can be used for moderately thick orthotropic beams. Many refined beam models have been developed over the last decades to extend the application of beam models to problems characterized by out-of-plane warping, in-plane distortions, torsion, coupling effects, or local effects. These effects are usually due

to small slenderness ratios, thin walls, geometrical and mechanical asymmetries, and the anisotropy of the material.
Many methods have been proposed to enhance the capabilities of beam models and preserve their computational efficiency. Several examples of these models can be found in well-known books on the theory of elasticity, for example, the book by Novozhilov [5]. Some of the most important methodologies are the following [6]:

- The introduction of shear correction factors [7, 8, 9].
- Warping functions [10, 11, 12, 13].
- Saint-Venant based 3D solutions [14] and the Proper Generalized Decomposition method (PGD) [15, 16].
- The Variational Asymptotic Beam Sectional Analysis (VABS), which is based on the Variational Asymptotic Method (VAM) [17, 18].
- The Generalized Beam Theory (GBT) [19, 20].
- Higher-Order expansions [21, 22, 23, 24].
- The Carrera Unified Formulation (CUF) [25].

Most of these models were developed for metallic structures and then extended to composites. Well-known examples are those by Reddy [26, 27], Surana [28], Kameswara Rao [29], Qatu [30], Eisenberger [31], Vidal [32], Shimpi [33], and Onate [34]. A comprehensive review can be found in [22, 23]. The present work presents an innovative approach based on the CUF. The CUF is a hierarchical formulation that can be used to reduce 3D problems to 2D or 1D ones in a unified manner by exploiting arbitrary rich expansions of the unknown variables. The main advantage and novelty of CUF models stems from the possibility of setting the order of the theory as an input of the analysis. The proper theory order is chosen via a convergence analysis for a given problem. CUF was first developed for plates and shells [35, 36] and more recently for beams [37, 38]. In the last years, CUF 1D models have been successfully extended to many structural problems, including:

- Thin-walled [39, 40] and reinforced structures [41, 42].
- Buckling [43], free vibration [44, 45, 46], dynamic response analysis [47] and aeroelasticity [48, 49, 50].
- Composite [51, 52, 53, 54, 55], functionally graded material (FGM)[56, 57] and nano-structures [58].
- Variable kinematics [59, 60] and axiomatic/asymptotic analyses [61, 62].
- Load factors and non-structural masses [63, 64, 65].
- Rotors and rotating blades [66, 67, 68].
- Biomechanics [69] and multifield analysis [70, 71].
- Aerospace [72] and civil [73, 74] strictures.

This work presents an overview of the most recent developments in the Component-Wise approach (CW). The CW can be seen as an extension of 1D CUF and can be straightforwardly obtained by using Lagrange polynomials to model the cross-section displacement field. In a CW model, each component of a complex structure is modeled through 1D models. Lagrange polynomials make the assembling of each component straightforward since it can be conducted at the interface level by imposing the displacement continuity. Furthermore, 1D, 2D, and 3D structural elements can be modeled through 1D models by enriching the displacement fields. The definition of mathematical lines and surfaces is no more needed since the unknown variables can be placed on the physical surfaces of the structure. CW models have been recently exploited to deal with:

- Analysis of aerospace structures [75, 76, 65, 77, 78].
- Analysis of civil structures [79, 80].
- Analysis of fiber/matrix cells of composite structures [81, 82].
- Damage analysis [83].

This work is organized as follows: the CUF and CW are first introduced; numerical examples on civil, aerospace and composite structures are then shown and discussed; the main conclusions and perspectives are drawn.

Carrera Unified Formulation

Let us assume the Cartesian, orthogonal coordinate frame shown in Fig. 1. In the CUF framework, a 1D structural model can be built according to the following unified displacement field:

$$\mathbf{u}(x,y,z) = F_\tau(x,z)\mathbf{u}_\tau(y), \qquad \tau = 1,2,....,M \tag{1}$$

where $\mathbf{u}(x,y,z) = \{u_x, u_y, u_z\}^T$ is the displacement vector; $F_\tau(x,z)$ indicates the cross-section functions; $\mathbf{u}_\tau$ is the generalized displacement vector; M indicates the number of terms in the expansion. The repeated subscript indicates summation. The choice of F_τ and M is arbitrary. In other words,

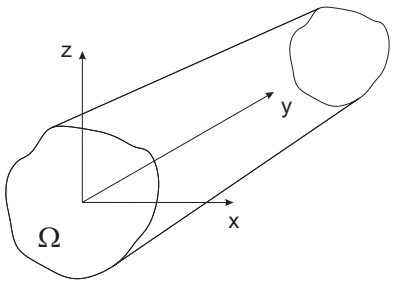

Fig. 1: Coordinate frame.

various types of basis functions can be used to model the displacement field across the section - e.g. polynomials, harmonics, exponentials, and combinations thereof - as well as any expansion orders.

The first 1D CUF model was developed using Taylor-like polynomial expansions and is referred to as TE. For example, the displacement field of the second-order TE model can be expressed as follows:

$$\begin{aligned} u_x(x,y,z) &= u_{x_1}(y) + x\ u_{x_2}(y) + z\ u_{x_3}(y) + x^2\ u_{x_4}(y) + xz\ u_{x_5}(y) + z^2\ u_{x_6}(y) \\ u_y(x,y,z) &= u_{y_1}(y) + x\ u_{y_2}(y) + z\ u_{y_3}(y) + x^2\ u_{y_4}(y) + xz\ u_{y_5}(y) + z^2\ u_{y_6}(y) \\ u_z(x,y,z) &= u_{z_1}(y) + x\ u_{z_2}(y) + z\ u_{z_3}(y) + x^2\ u_{z_4}(y) + xz\ u_{z_5}(y) + z^2\ u_{z_6}(y) \end{aligned} \tag{2}$$

Where the parameters on the right-hand side (u_{x_1}, u_{y_1}, u_{z_1}, u_{x_2}, etc.) represent the components of the generalized displacement vector. Such a model is referred to as $N = 2$, where N indicates the order of the expansion.

LE models are based on Lagrange polynomial expansions. Each set of Lagrange polynomials is referred to as L-element. In this work, mainly bi-quadratic nine-nodes (L9) Lagrange polynomials are used as F_τ. Lagrange polynomials can be found in [38]. The displacement field within an L9 element can be written as:

$$\begin{aligned} u_x(x,y,z) &= F_1(x,z)u_{x1}(y) + F_2(x,z)u_{x2}(y) + ... + F_9(x,z)u_{x9}(y) \\ u_y(x,y,z) &= F_1(x,z)u_{y1}(y) + F_2(x,z)u_{y2}(y) + ... + F_9(x,z)u_{y9}(y) \\ u_z(x,y,z) &= F_1(x,z)u_{z1}(y) + F_2(x,z)u_{z2}(y) + ... + F_9(x,z)u_{z9}(y) \end{aligned} \tag{3}$$

Where $u_{x1}, ..., u_{z9}$ are the translational components of the nine points of the L9 element. The unknown variables are only pure displacements. Figure 2 shows a typical L9 distribution above a cross-section with local loads. The local refinement of the displacement field is achieved via the use of a finer discretization. Arbitrary geometries can be dealt with via the iso-parametric formulation. Figure 3

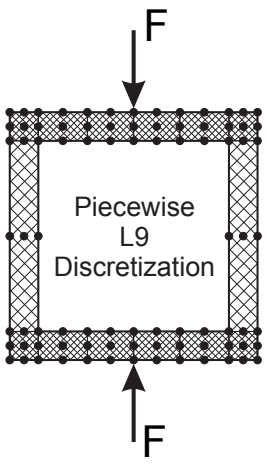

Fig. 2: L9 element distribution above a cross-section undergoing local loads.

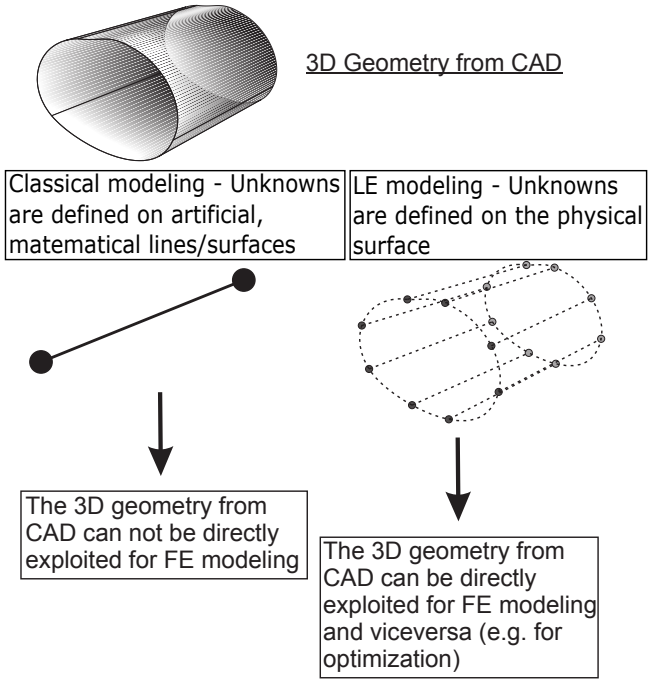

Fig. 3: Classical and LE modeling strategies with respect to the 3D geometry.

shows the LE capability of using directly the physical surfaces of the structure to place the unknown variables. In other words, while classical models and TE require the definition of a line - commonly known as the beam axis - along which the unknown variables are defined, LE can use the physical boundaries of the 3D body. Such a feature can be of fundamental importance whenever a 3D CAD geometry must be dealt with.

Geometrical and Constitutive Equations The stress σ and the strain ϵ vectors are defined as follows:

$$\begin{aligned} \boldsymbol{\sigma} &= \{\sigma_{xx}, \sigma_{yy}, \sigma_{zz}, \sigma_{xy}, \sigma_{xz}, \sigma_{yz}\}^T \\ \boldsymbol{\epsilon} &= \{\epsilon_{xx}, \epsilon_{yy}, \epsilon_{zz}, \epsilon_{xy}, \epsilon_{xz}, \epsilon_{yz}\}^T \end{aligned} \tag{4}$$

The linear strain-displacement relations are employed,

$$\boldsymbol{\epsilon} = \boldsymbol{D}\boldsymbol{u} \tag{5}$$

where $\boldsymbol{D}$ is

$$\boldsymbol{D} = \begin{bmatrix} \frac{\partial}{\partial x} & 0 & 0 \\ 0 & \frac{\partial}{\partial y} & 0 \\ 0 & 0 & \frac{\partial}{\partial z} \\ \frac{\partial}{\partial y} & \frac{\partial}{\partial x} & 0 \\ \frac{\partial}{\partial z} & 0 & \frac{\partial}{\partial x} \\ 0 & \frac{\partial}{\partial z} & \frac{\partial}{\partial y} \end{bmatrix} = \begin{bmatrix} \frac{\partial}{\partial x} & 0 & 0 \\ 0 & 0 & 0 \\ 0 & 0 & \frac{\partial}{\partial z} \\ 0 & \frac{\partial}{\partial x} & 0 \\ \frac{\partial}{\partial z} & 0 & \frac{\partial}{\partial x} \\ 0 & \frac{\partial}{\partial z} & 0 \end{bmatrix} + \begin{bmatrix} 0 & 0 & 0 \\ 0 & \frac{\partial}{\partial y} & 0 \\ 0 & 0 & 0 \\ \frac{\partial}{\partial y} & 0 & 0 \\ 0 & 0 & 0 \\ 0 & 0 & \frac{\partial}{\partial y} \end{bmatrix} = [\boldsymbol{D}_\Omega] + [\boldsymbol{D}_y] \tag{6}$$

The constitutive law is

$$\boldsymbol{\sigma} = \tilde{\boldsymbol{C}}\boldsymbol{\epsilon} \tag{7}$$

For the sake of brevity, the coefficients of $\tilde{\boldsymbol{C}}$ are non reported here, they can be found in Reddy's book [84].

Finite Element Formulation and the Fundamental Nucleus The generalised displacement vector $\mathbf{u}_\tau$ is interpolated along the y direction by means of the shape functions N_i,

$$\boldsymbol{u}(x, y, z) = F_\tau(x, z) N_i(y) \boldsymbol{u}_{\tau i} \tag{8}$$

where $\mathbf{u}_{\tau i}$ is the nodal unknown vector. According to the principle of virtual displacements, the internal strain energy L_{int} can be written as follows:

$$\delta L_{int} = \int_V \delta\boldsymbol{\epsilon}^T \boldsymbol{\sigma}\, dV \tag{9}$$

Where δ stands for virtual variation. Considering Eqs. 5, 7 and 8, the virtual variation of the strain energy can be written in a compact form:

$$\delta L_{int} = \delta \boldsymbol{u}_{sj}^T \mathbf{K}^{\tau sij} \boldsymbol{u}_{\tau i} \tag{10}$$

where $\mathbf{K}^{\tau sij}$ is the fundamental nucleus of the stiffness matrix and the superscripts indicate the four indexes exploited to expand the elemental matrix: τ and s are related to the expansion functions F_τ and F_s whereas *i* and *j* are related to the shape functions N_i and N_j.

The fundamental nucleus, which is a 3x3 array, is formally independent of the order of the beam model. By introducing the geometrical and constitutive relations, it is possible to rewrite the virtual variation of L_{int} as

$$\begin{aligned}\delta L_{int} = \delta \mathbf{u}_{sj}^T \Bigg\{ \int_V \Big[\Big(\boldsymbol{D}_\Omega + \boldsymbol{D}_y\Big)^T \Big(F_s(x,z) N_j(y) \boldsymbol{I}\Big)\Big] \boldsymbol{C} \Big[\Big(\boldsymbol{D}_\Omega + \boldsymbol{D}_y\Big)\Big(N_i(y) F_\tau(x,z) \boldsymbol{I}\Big)\Big] dV \Bigg\} \mathbf{u}_{\tau i} = \\ = \delta \mathbf{u}_{sj}^T \Bigg\{ \int_l \Big(N_j(y) \Big(\int_\Omega \Big[\boldsymbol{D}_\Omega^T \Big(F_s(x,z)\boldsymbol{I}\Big)\Big] \boldsymbol{C} \Big[\boldsymbol{D}_\Omega \Big(F_\tau(x,z)\boldsymbol{I}\Big)\Big] d\Omega \Big) N_i(y)\Big) dy + \\ + \int_l \Big(N_j(y) \Big(\int_\Omega \Big[\boldsymbol{D}_\Omega^T \Big(F_s(x,z)\boldsymbol{I}\Big)\Big] \boldsymbol{C} F_\tau(x,z) d\Omega \Big) \boldsymbol{D}_y \Big(N_i(y)\boldsymbol{I}\Big)\Big) dy + \\ + \int_l \Big(\boldsymbol{D}_y^T \Big(N_j(y)\boldsymbol{I}\Big) \Big(\int_\Omega F_s(x,z) \boldsymbol{C} \Big[\boldsymbol{D}_\Omega \Big(F_\tau(x,z)\boldsymbol{I}\Big)\Big] d\Omega \Big) N_i(y)\Big) dy + \\ + \int_l \Big(\boldsymbol{D}_y^T \Big(N_j(y)\boldsymbol{I}\Big) \Big(\int_\Omega F_s(x,z) \boldsymbol{C} F_\tau(x,z) d\Omega \Big) \boldsymbol{D}_y \Big(N_i(y)\boldsymbol{I}\Big)\Big) dy \Bigg\} \mathbf{u}_{\tau i}\end{aligned} \tag{11}$$

where Ω is the cross-section domain and $\mathbf{I}$ is the unit matrix. All the other finite element matrices and vectors can be written in a similar way, as shown in [38].

The Component-Wise Approach

The advanced capabilities of CUF 1D models can be particularly convenient in the case of multi-component structures (MCS). MCS represent most of the engineering structures. Typical examples are aircraft wings and composite structures. These structures are composed of multiple components, which can have quite different geometrical and material characteristics. In a wing structure, for instance, ribs and panels can be modelled as plates or shells (2D), while stiffeners or spars can be modeled as beams (1D) or solids (3D). An efficient FE modelling of MCS often requires the coupling of different elements – beams/shells/solids – to build sufficiently accurate models with a reasonable number of DOFs.

A fibre reinforced composite plate is made of layers composed of matrix and fibers. In most cases, such plates can be modeled as homogenized structures through the equivalent single layer (ESL) and layer-wise (LW) approaches. The former models a multilayered plate as an equivalent monolayer plate. The latter retains each layer but with higher computational costs. Recently, multiscale approaches have been proposed to model composites up to the fiber and matrix level. Such approaches are necessary to retain the microscale characteristics and to model processes occurring at a certain scale and influencing the behavior of the system across several scales. A typical example of a multiscale problem is failure analysis. Several multiscale approaches have been proposed in the last years, but their utilization is still challenging due to their computational costs. A multiscale model can, in fact, easily have millions of DOFs.

The CW exploits LE 1D elements to model each component of a structure separately and independently of their geometrical and material characteristics. In other words, each 1D, 2D, 3D or micro and macro component can be modeled via LE 1D models with no need for ad hoc coupling and interface techniques. Figure 4(a) shows the CW approach for a four-stringer wing box. Each component of the box is modelled using LE cross-sectional elements. In particular,

- Ribs are modeled as very short beams via refined displacement fields.

- Each component geometrical and material characteristics are retained.
- The CW approach does not require coupling techniques, as the FE matrices of each element are formally the same. This process usually leads to inaccuracies whenever beams, plates, shells, and solids have to be interfaced.

CW models can be locally refined by using higher- or lower-order models where required. Such a feature leads to further computational cost reductions.
CW can also lead to multiscale modeling. Figure 4(b) shows a typical CW strategy for a composite plate; 1D LE models can be simultaneously adopted to model layers (macroscale), matrix and fibres (microscale). This methodology can be very powerful when, for instance, detailed stress fields are required in a specific portion of the structures. Figure 5 shows the different assemblage strategies for a multicomponent structure stiffness matrix. In classical approaches, the structure is reduced to a single equivalent structure. In the CW, the stiffness matrix elements of different components are superimposed only at the interface level to impose the displacement continuity.

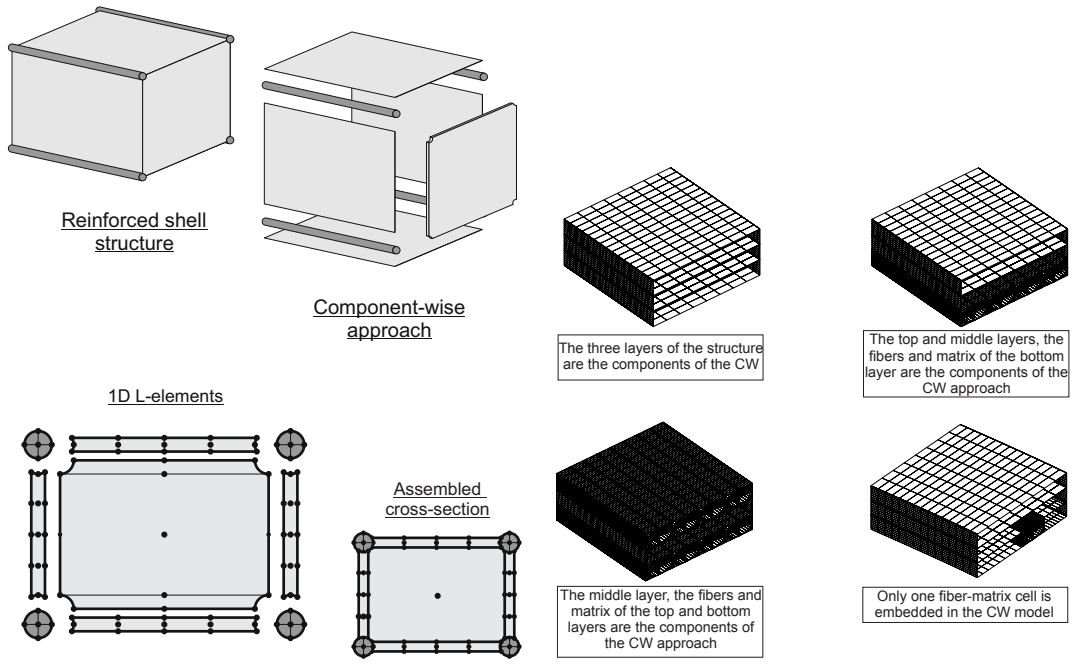

(a) A reinforced shell structure for aerospace applications

(b) A fiber reinforced composite structure

Fig. 4: CW modeling of multi-component structures.

Numerical Examples

Static Analysis of Civil Structures A two-bay truss structure with transverse stiffeners was considered as the first example, see Fig. 6. The dimensions of the structure are: $h = w = 0.2$ m, $t = 0.02$ m, $L = 2$ m. A steel alloy was employed, $E = 210$ GPa and $\nu = 0.29$. A vertical point load, $F_z = -100$ N, was applied at the middle-span transverse stiffener at $x = 0$, $z = h/2$. Hinged supports were used. Figure 7 shows three different modeling strategies. Model A exploits a combination of L3, L4 and L9 elements. In particular, L4 were used for the stringers. In Model B, L3 and L9 were used on the cross-section of the stiffener, whereas L9 elements were used for the longitudinal frames. Model C has the same discretization scheme of Model B, but two L9 were used on the cross-section of the horizontal and vertical frames. Table 1 shows the results in terms of transverse displacement. CW models were compared with beam and solid models. Figure 8 shows the deformed

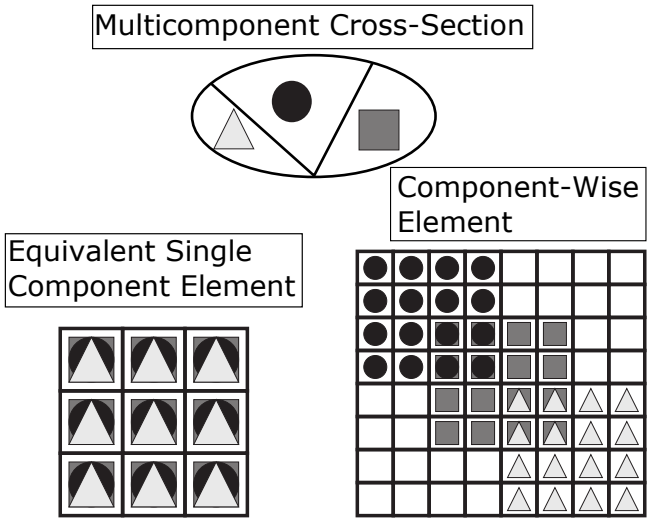

Fig. 5: Stiffness matrix assemblage schemes.

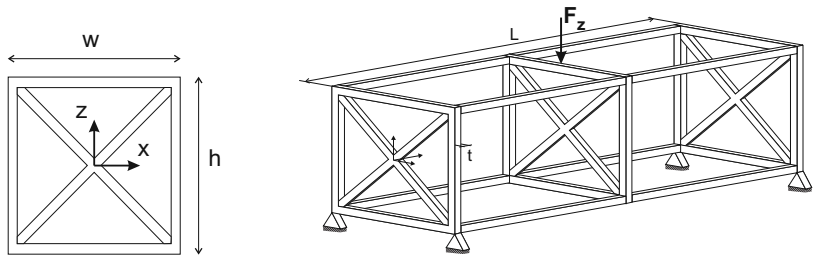

(a) Cross-Section (b) Boundary Conditions

Fig. 6: Two-bay truss structure.

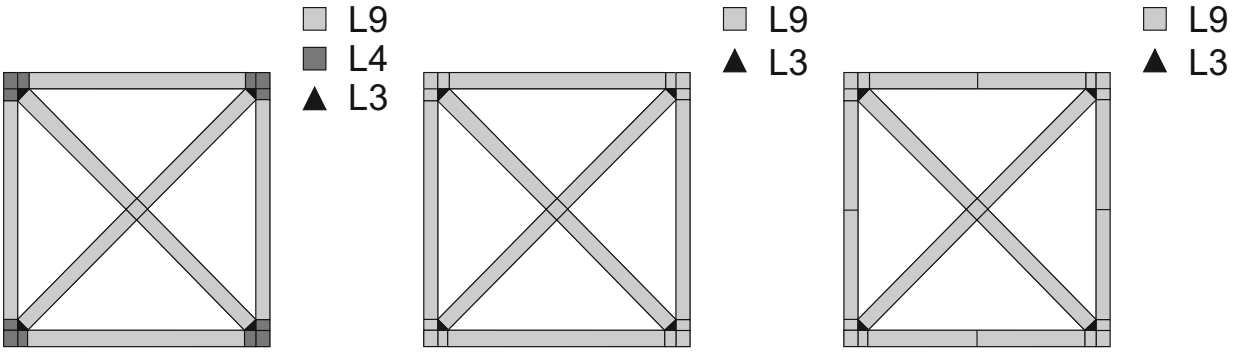

(a) Model A (b) Model B (c) Model C

Fig. 7: Cross-Sectional L-element distributions for the truss structure.

configuration of the structure obtained by the CW model. A typical industrial frame was considered as the second example, see Fig. 9 and Table 2. Columns and frames have a square cross-section with side $t = 0.2$ m. The thickness of the roof is equal to t. A horizontal load, $F_x = -2000$ N, was applied. The CW model is based on a beam laying along the y-axis. Figure shows the L-element distribution above the cross-section of the structure. The sole difference between Model A and B is that 4 L9 instead of 2 L9 elements were used in Model B to discretize the columns to highlight local enrichment capability of CW. Nastran models were employed for comparison purposes. A full solid model and an FE model obtained by using a combination of 1D beam - 2-node CBAR beam elements to model columns and

Table 1: Vertical displacement at $[0, L/2, h/2]$ for the two-bay truss structure [79].

Model	$-u_z$, mm	DOFs
	CW	
Model A	0.880	3828
Model B	1.015	6732
Model C	1.026	7596
	Nastran	
Beam	1.065	7562
Solid	1.050	98760

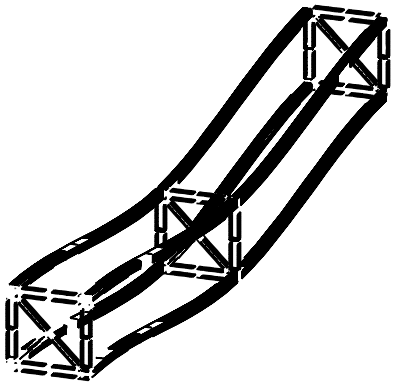

Fig. 8: Deformed two-bay truss structure, Model C.

frame - and 2D plate elements (CQUAD) for the roof. Table 3 shows the displacement and the number of DOFs for each model. Figure 11 shows the deformed structure.

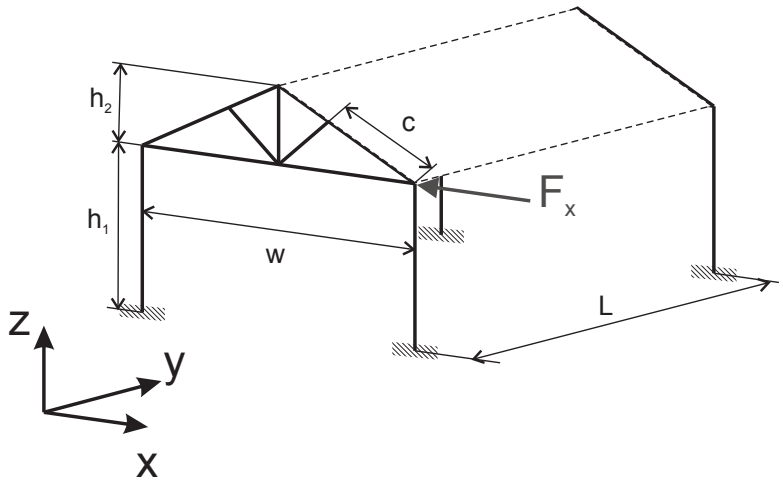

Fig. 9: Industrial frame.

Table 2: Dimensions of the industrial frame

	Dimensions, m
L	14.00
w	13.80
h_1	7.00
h_2	3.00
c	4.50

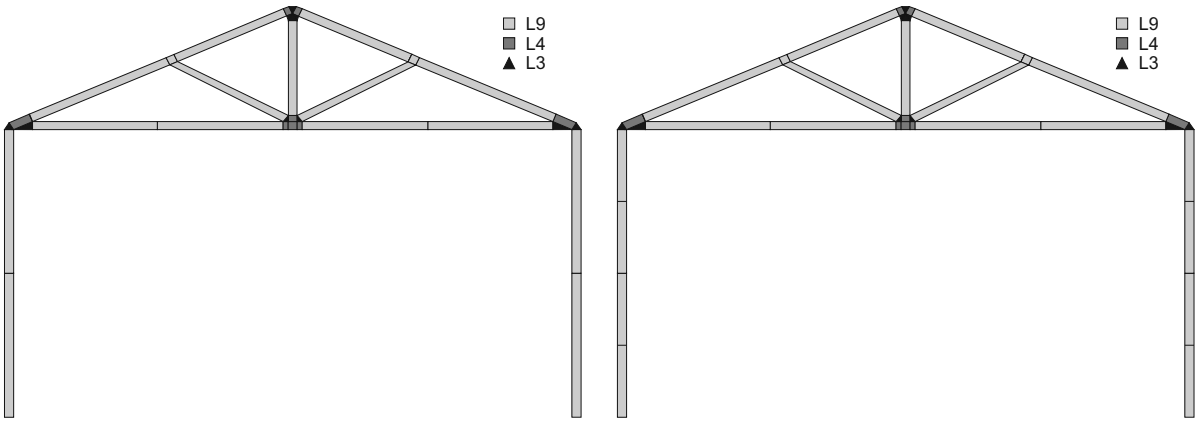

(a) Model A (b) Model B

Fig. 10: Cross-Sectional L-element distributions for the industrial frame.

Table 3: Displacements for the industrial frame at the load application point [79].

Model	$-u_x$, mm	DOFs
	CW	
Model A	0.713	6543
Model B	0.893	7119
	Nastran	
Beam/Shell	0.865	2835
Solid	0.858	143121

.

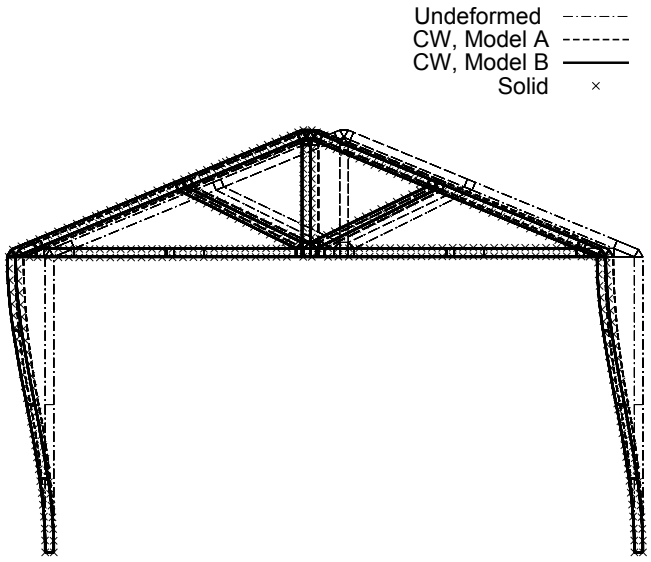

Fig. 11: Deformed industrial frame.

The results suggest that

- The CW can analyse truss and frame structures, including stiffening members and panels.
- The CW results match Nastran ones.
- In particular, CW provides solid-like accuracies with very low computational costs.
- The computational efficiency of the proposed CW models is given not only by low computational costs. The CW models each structural component - columns, frame members, and roof - with the same 1D element and different kinematics are not needed. Moreover, artificial lines (beam axes) and surfaces (plate/shell reference surfaces) are no longer used. This is otherwise possible only if 3D solid elements are adopted.

Dynamic Response of Aircraft Wings A metallic aircraft wing is considered in this section. A NACA 2415 airfoil cross-section was used with two longerons. The wing is 6 m long, and the chord is 1 m. Figure 12 shows the configurations analysed. To analyse the behaviour of a thin-walled structure, the model was modified by removing ribs and longerons, as in Fig. 12(b). Moreover, the effect of the presence of an open bay was evaluated, as in Fig. 12(c). Aluminum was used, $E = 75$ GPa, $\nu = 0.33$ and $\rho = 2770$ Kg/m^3. L9 elements were used to discretize the cross-section. A vertical harmonic load was applied at $y = 1.996$ m on the second longeron, $F = 1000$ N and $\omega = 3$ rad/s. The modal superposition method was used to compute the time-dependent response. Table 4 shows the transverse displacements obtained via classical models and the CW. Figure 13 shows the time-dependent displacement of the leading edge and the trailing edge of the configurations A and C.
The results suggest that

- Classical and CW models provide same results for the configuration A.
- In B and C, local effects take place and torsion is more evident. Both behaviors make the differences between classical and CW models higher.

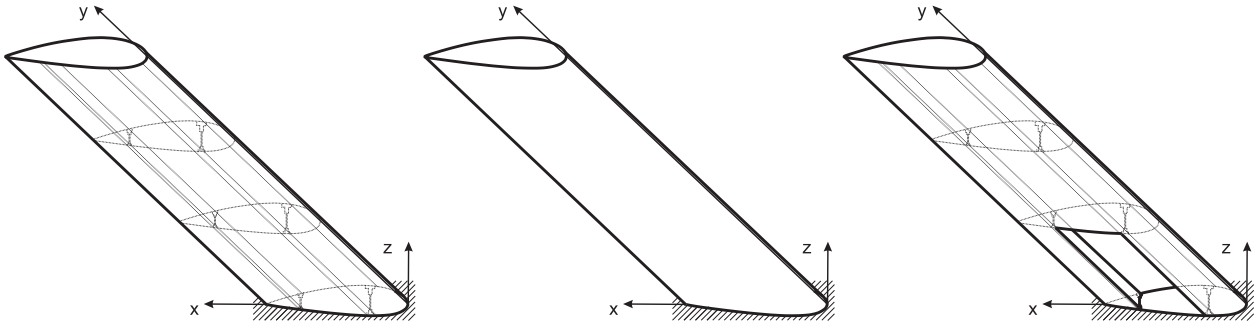

(a) Configuration A : Complete Wing (b) Configuration B : Skin Only (c) Configuration C : Open Bay

Fig. 12: Wing configurations.

Table 4: Maximum and minimum u_z displacement (mm) at the tip of the wing obtained by means of different theories [77].

Point		EBBT	TBT	LE
Configuration A				
DOFs		84	140	24864
Leading Edge	$u_{z_{max}}$	6.036	6.045	5.711
	$u_{z_{min}}$	−6.183	−6.198	−5.866
Trailing Edge	$u_{z_{max}}$	6.036	6.045	6.102
	$u_{z_{min}}$	−6.183	−6.198	−6.261
Configuration B				
DOFs		84	140	14616
Leading Edge	$u_{z_{max}}$	8.591	8.593	8.211
	$u_{z_{min}}$	−8.696	−8.711	−8.277
Trailing Edge	$u_{z_{max}}$	8.591	8.593	9.213
	$u_{z_{min}}$	−8.696	−8.711	−9.299
Configuration C				
DOFs		84	140	24450
Leading Edge	$u_{z_{max}}$	8.319	8.318	7.690
	$u_{z_{min}}$	−7.879	−7.889	−7.253
Trailing Edge	$u_{z_{max}}$	8.319	8.318	9.084
	$u_{z_{min}}$	−7.879	−7.889	−8.594

Damaged Beam A cantilever I-beam was considered. The beam length is 1 m, the height and width of the cross-section are 0.1 m, and the thickness of the flanges is 0.002 m. The material is isotropic; E = 75 GPa, ν = 0.33, and ρ = 2700 Kg/m^3. Various damage distributions along the cross-section were employed, as shown in Fig. 14 and Table 5. The damage was introduced along the 10% of the length, from the root onwards. d indicates the degradation rate of the Young modulus, that is, $E_d = d \times E$. Figure 15 shows the first five frequencies of the beam. Classical models, TE, and

Table 5: Damage distribution above the cross-section of the I-beam.

	A	B	C	D	E
Set 1, d =	0.5	0.7	0.8	0.6	0.9
Set 2, d =	0.1	0.7	0.1	0.6	0.9

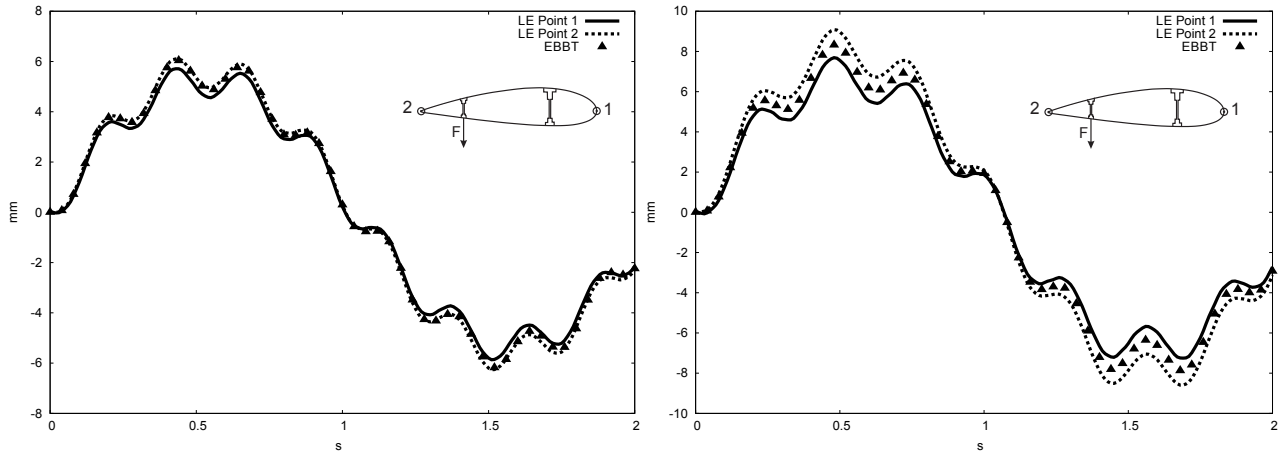

(a) Configuration A (b) Configuration C

Fig. 13: Time-dependent transverse displacement of the wing at the tip for various theories.

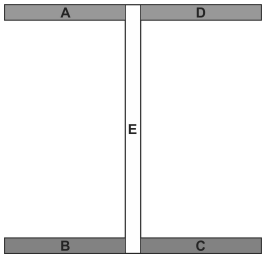

Fig. 14: Cross-section of the I-beam.

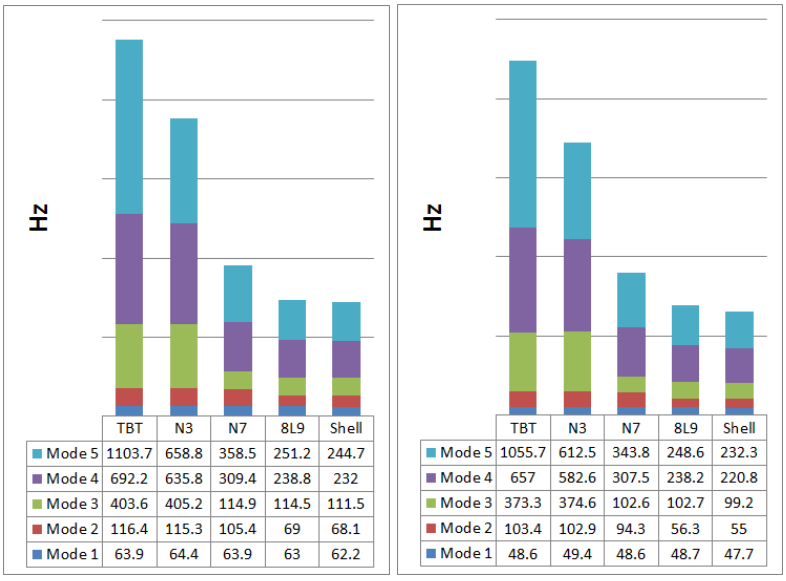

	TBT	N3	N7	8L9	Shell
Mode 5	1103.7	658.8	358.5	251.2	244.7
Mode 4	692.2	635.8	309.4	238.8	232
Mode 3	403.6	405.2	114.9	114.5	111.5
Mode 2	116.4	115.3	105.4	69	68.1
Mode 1	63.9	64.4	63.9	63	62.2

(a) Set 1

	TBT	N3	N7	8L9	Shell
Mode 5	1055.7	612.5	343.8	248.6	232.3
Mode 4	657	582.6	307.5	238.2	220.8
Mode 3	373.3	374.6	102.6	102.7	99.2
Mode 2	103.4	102.9	94.3	56.3	55
Mode 1	48.6	49.4	48.6	48.7	47.7

(b) Set 2

Fig. 15: First five natural frequencies of the I-beam [83].

LE were used. Moreover, a shell model was exploited for comparison purposes. LE and shell provide the same results. Classical models are inadequate because the first five modes of both structures have either bending-torsion couplings of severe shell-like phenomena, as shown in Fig. 16. The presence of damage introduces local phenomena that cannot be detected by classical models. TE models can deal with such phenomena but with high order expansions ($N > 7$).

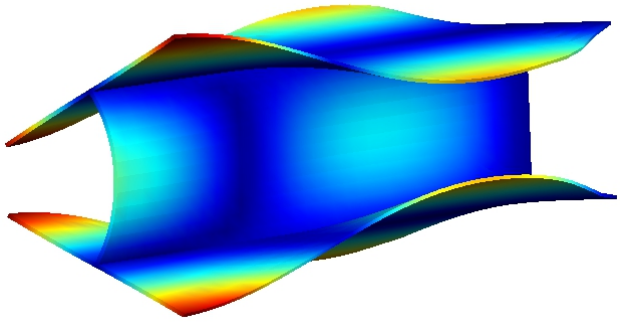

Fig. 16: Fifth mode of the I-beam, set 2.

Damaged Fiber/Matrix Cells The CW can be used to model fiber/matrix cells as shown in Fig. 17. Such a modeling approach could be used locally or in a multiscale scenario to have very accurate stress fields with low computational costs. This section shows the results of the free vibration analysis of a cell via different CW models and 3D solids. The cell length is 40 mm; the height is 0.6 mm, and

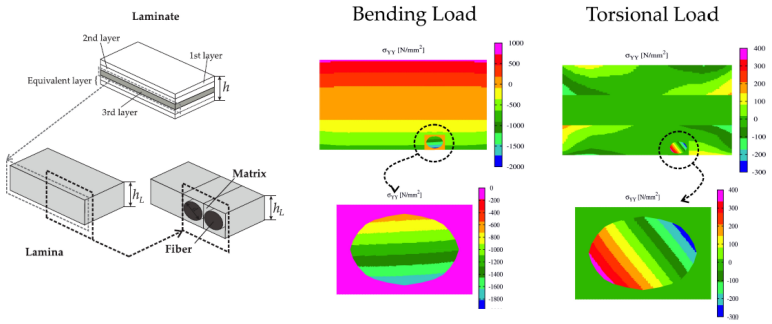

Fig. 17: Component-Wise model of a laminated plate.

the width is 0.8 mm. One end of the structure is clamped. A $0/90/0$ lamination was considered. Figure 18 shows the four modeling approaches adopted. Fibers were modeled with a circular cross-section, where the diameter is equal to 0.2 mm. Fibers are orthotropic, with $E_L = 202.038$ GPa, $E_T = E_Z = 12.134$ GPa, $G_{LT} = G_{LZ} = 8.358$ GPa, $G_{TZ} = 47.756$ GPa, $\nu_{LT} = \nu_{LZ} = 0.2128$ und $\nu_{TZ} = 0.2704$. The matrix is made of an isotropic material, with $E = 3.252$ GPa and $\nu = 0.355$. Layer properties are orthotropic and are as the following: $E_L = 159.380$ GPa, $E_T = E_Z = 14.311$ GPa, $G_{LT} = G_{LZ} = 3.711$ GPa, $G_{TZ} = 5.209$ GPa, $\nu_{LT} = \nu_{LZ} = 0.2433$ und $\nu_{TZ} = 0.2886$. The density, ρ, is 1300 kg/m^3, 1500 kg/m^3 and 1555 kg/m^3 are adopted for the matrix, layer, and fiber, respectively. Mixture rules were used. The bottom layer was damaged along the first 10% of the span. The damage was modeled by the degradation of Young and shear moduli.

Table 6 shows the first five natural frequencies of the structure for various damage levels. CW models obtained through LEs were compared to solid FE models (Abaqus). Bending and torsional modes were considered. The total amount of degrees of freedom (DOFs) for each model is given in the last row. A good match between the two models was found.

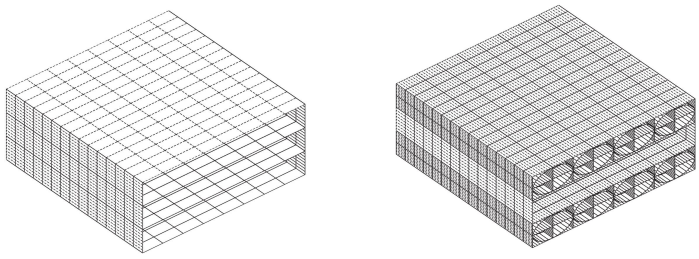

(a) Model 1: the three layers of the structure are the components of the CW approach

(b) Model 2: the top and middle layers and the fibers and matrices of the bottom layer are the components of the CW approach

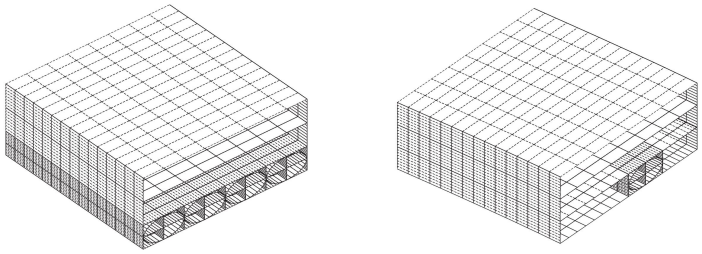

(c) Model 3: the middle layer and the fibers and matrices of the top and bottom layers are the components of the CW approach

(d) Model 4: only one fiber-matrix cell is inserted in CW model

Fig. 18: Various modeling approaches for the laminate.

.

Table 6: First five natural frequencies (Hz).

	Model 1							
	$d = 0.1$		$d = 0.5$		$d = 0.9$		$d = 1.0$	
	CW	Solid	CW	Solid	CW	Solid	CW	Solid
Mode 1	420.49^{b}	412.45^{b}	568.05^{b}	562.66^{b}	607.25^{b}	601.84^{b}	613.01^{b}	607.56^{b}
Mode 2	609.17^{b}	603.90^{b}	657.13^{b}	651.82^{b}	687.32^{b}	681.81^{b}	693.29^{b}	687.75^{b}
Mode 3	3248.2^{b}	3211.4^{b}	3629.3^{b}	3597.1^{b}	3776.3^{b}	3744.1^{b}	3800.2^{b}	3767.8^{b}
Mode 4	3985.1^{b}	3954.2^{b}	4132.6^{b}	4101.0^{b}	4246.4^{b}	4214.0^{b}	4271.0^{b}	4238.5^{b}
Mode 5	8169.3^{t}	7903.9^{t}	8743.2^{t}	8503.6^{t}	8964.4^{t}	8724.0^{t}	9000.8^{t}	8759.7^{t}
DOFs	5859	75789	5859	75789	5859	75789	5859	75789
	Model 2							
Mode 1	409.74^{b}	458.34^{b}	557.89^{b}	589.92^{b}	596.51^{b}	628.08^{b}	602.15^{b}	606.92^{b}
Mode 2	599.46^{b}	624.55^{b}	648.81^{b}	671.44^{b}	678.95^{b}	701.59^{b}	684.86^{b}	687.77^{b}
Mode 3	3144.1^{b}	3412.1^{b}	3512.2^{b}	3764.6^{b}	3653.3^{b}	3908.4^{b}	3676.1^{b}	3766.5^{b}
Mode 4	3941.2^{b}	4086.9^{b}	4094.4^{b}	4235.6^{b}	4209.3^{b}	4350.8^{b}	4233.8^{b}	4254.5^{b}
Mode 5	7599.4^{t}	9046.3^{t}	8084.4^{t}	9738.6^{t}	8290.0^{t}	9984.4^{t}	8324.7^{t}	10187^{t}
DOFs	16275	92346	16275	92346	16275	92346	16275	92346
	Model 3							
Mode 1	417.06^{b}	420.13^{b}	563.22^{b}	566.17^{b}	601.91^{b}	604.98^{b}	607.58^{b}	608.44^{b}
Mode 2	605.38^{b}	608.16^{b}	653.52^{b}	654.90^{b}	683.2^{b}	684.66^{b}	689.10^{b}	687.67^{b}
Mode 3	3195.7^{b}	3238.8^{b}	3568.7^{b}	3618.1^{b}	3713.89^{b}	3764.0^{b}	3737.5^{b}	3773.7^{b}
Mode 4	3968.3^{b}	3976.9^{b}	4115.6^{b}	4124.3^{b}	4227.91^{b}	4238.2^{b}	4252.1^{b}	4244.0^{b}
Mode 5	7903.3^{t}	8612.5^{t}	8403.6^{t}	9303.5^{t}	8619.94^{t}	9536.0^{t}	8656.7^{t}	9497.5^{t}
DOFs	9765	268440	9765	268440	9765	268440	9765	268440
	Model 4							
Mode 1	420.11^{b}	436.18^{b}	567.41^{b}	577.96^{b}	606.50^{b}	616.97^{b}	612.24^{b}	612.01^{b}
Mode 2	608.85^{b}	616.76^{b}	656.61^{b}	664.37^{b}	686.70^{b}	694.57^{b}	692.66^{b}	692.12^{b}
Mode 3	3244.21^{b}	3318.8^{b}	3624.74^{b}	3689.9^{b}	3771.46^{b}	3836.4^{b}	3795.3^{b}	3794.7^{b}
Mode 4	3982.42^{b}	4030.7^{b}	4129.66^{b}	4178.7^{b}	4243.23^{b}	4293.1^{b}	4267.8^{b}	4266.6^{b}
Mode 5	8171.29^{t}	8238.5^{t}	8745.96^{t}	8837.0^{t}	8966.89^{t}	9061.1^{t}	9003.2^{t}	9106.2^{t}
DOFs	11811	60282	11811	60282	11811	60282	11811	60282

$(^{*})$: b, t refer to bending and torsional mode, respectively.

Conclusion

This work has presented the Component-Wise approach for the structural modeling of civil, aerospace and composite structures. The Carrera Unified Formulation has been briefly introduced together with its extensions to the CW. The main features of CW are the following:

- 1D CUF models are used as structural models. In particular, Lagrange expansions (LE) are used to define the displacement field above the cross-section. 1D CUF models can be refined to an arbitrary extent and can be used to analyse 2D and 3D structures as well.

- No artificial, mathematical lines and surfaces are needed. The problem unknowns are, in fact, placed on the physical surface of the 3D structure.
- No homogenization techniques of the material characteristics nor interface techniques of different components are needed.

Particular attention has been paid to the analysis of multi-component structures in which 1D, 2D and 3D components have been modeled via 1D finite elements only. Moreover, preliminary analyses aimed at the multiscale analysis of composite structures have been presented. The results have confirmed the enhanced capabilities of the CW in terms of 3D-like accuracies and low computational costs.
The CW approach may have interesting future extensions due to its inherent advanced capabilities. In particular, the CW may be extended to many of those problems in which very accurate 3D stress fields are needed but are often difficult to deal with due to extremely high computational costs. Typical examples are the following:

- Damage and progressive failure analyses.
- Multiscale analyses.
- Impact problems.
- Health-monitoring.
- Biomedical fluid-structure interaction problems.

References

[1] D. Bernoulli. *Commentarii Academiae Scientiarum Imperialis Petropolitanae*, chapter De vibrationibus et sono laminarum elasticarum. Petropoli, 1751.

[2] L. Euler. *De curvis elasticis*, chapter Methodus Inveniendi Lineas Curvas Maximi Minimive Proprietate Gaudentes, Sive Solutio Problematis Isoperimetrici Lattissimo Sensu Accept. Bousquet, 1744.

[3] S. P. Timoshenko. On the corrections for shear of the differential equation for transverse vibrations of prismatic bars. *Philosophical Magazine*, 41:744–746, 1922.

[4] L. Da Vinci. *Codex Madrid*, volume I. 1493.

[5] V. V. Novozhilov. *Theory of Elasticity*. Pergamon Press, 1961.

[6] E. Carrera, A. Pagani, M. Petrolo, and E. Zappino. Recent developments on refined theories for beams with applications. *Mechanical Engineering Reviews*, 2(2):1–30, 2015. doi: 10.1299/mer.14-00298.

[7] G.R. Cowper. The shear coefficient in Timoshenko's beam theory. *Journal of Applied Mechanics*, 33(2):335–340, 1966.

[8] S.P. Timoshenko and J.N. Goodier. *Theory of elasticity*. McGraw-Hill, New York, 1970.

[9] I. S. Sokolnikoff. *Mathematical Theory of Elasticity*. McGraw-Hill, New York, 1956.

[10] A.A. Umanskij. *Kručenije i izgib tonkostennykh aviokon-strukcij*. Oborongiz, Moskva, 1939. (in Russian).

[11] V. Z. Vlasov. *Thin-walled elastic beams*. National Science Foundation, Washington, 1961.

[12] S. Benscoter. A theory of torsion bending for multicell beams. *Journal of Applied Mechanics*, 21(1):25–34, 1954.

[13] P. Ladevèze and J. Simmonds. New concepts for linear beam theory with arbitrary geometry and loading. *European Journal of Mechanics - A/Solids*, 17(3):377–402, 1998.

[14] P. Ladéveze and J. Simmonds. De nouveaux concepts en théorie des poutres pour des charges et des géométries quelconques. *Comptes Rendus Acad. Sci. Paris*, 332:445–462, 1996.

[15] B. Bognet, A. Leygue, and F. Chinesta. Separated representations of 3d elastic solutions in shell geometries. *Advanced Modeling and Simulation in Engineering Sciences*, 1(4), 2014. doi: 10.1186/2213-7467-1-4.

[16] P. Vidal, L. Gallimard, and O. Polit. Composite beam finite element based on the proper generalized decomposition. *Computers and Structures*, 102–103:76–86, 2012. doi: 10.1016/j.compstruc.2012.03.008.

[17] V.L. Berdichevsky. Equations of the theory of anisotropic inhomogeneous rods. *Dokl. Akad. Nauk*, 228:558–561, 1976.

[18] V.V. Volovoi, D.H. Hodges, V.L. Berdichevsky, and V.G. Sutyrin. Asymptotic theory for static behavior of elastic anisotropic I-beams. *International Journal of Solid Structures*, 36(7):1017–1043, 1999.

[19] R. Schardt. Eine erweiterung der technischen biegetheorie zur berechnung prismatischer faltwerke. *Der Stahlbau*, 35:161–171, 1966.

[20] N. Silvestre and D. Camotim. First-order generalised beam theory for arbitrary orthotropic materials. *Thin-Walled Structures*, 40(9):791–820, 2002.

[21] K. Washizu. *Variational Methods in Elasticity and Plasticity*. Pergamon, Oxford, 1968.

[22] K. Kapania and S. Raciti. Recent advances in analysis of laminated beams and plates, part I: Shear effects and buckling. *AIAA Journal*, 27(7):923–935, 1989.

[23] K. Kapania and S. Raciti. Recent advances in analysis of laminated beams and plates, part II: Vibrations and wave propagation. *AIAA Journal*, 27(7):935–946, 1989.

[24] L. Librescu and O. Song. On the static aeroelastic tailoring of composite aircraft swept wings modelled as thin-walled beam structures. *Composites Engineering*, 2:497–512, 1992.

[25] E. Carrera and G. Giunta. Refined beam theories based on a unified formulation. *International Journal of Applied Mechanics*, 2(1):117–143, 2010. doi: 10.1142/S1758825110000500.

[26] A.A. Khdeir and J.N. Reddy. Buckling of cross-ply laminated beams with arbitrary boundary conditions. *Composite Structures*, 37(1):1–3, 1997. doi: 10.1016/S0263-8223(97)00048-2.

[27] A.A. Khdeir and J.N. Reddy. An exact solution for the bending of thin and thick cross-ply laminated beams. *Composite Structures*, 37(2):195–203, 1997. doi: 10.1016/S0263-8223(97)80012-8.

[28] K.S Surana and S.H Nguyen. Two-dimensional curved beam element with higher-order hierarchical transverse approximation for laminated composites. *Computers and Structures*, 36(3):499–511, 1990. doi: 10.1016/0045-7949(90)90284-9.

[29] M. Kameswara Rao, Y.M. Desai, and M.R. Chitnis. Free vibrations of laminated beams using mixed theory. *Composite Structures*, 52(2):149–160, 2001. doi: 10.1016/S0263-8223(00)00162-8.

[30] M. S. Qatu. Theories and analyses of thin and moderately thick laminated composite curved beams. *International Journal of Solids and Structures*, 30(20):2743–2756, 1993. doi: 10.1016/0020-7683(93)90152-W.

[31] M. Eisenberger, H. Abramovich, and O. Shulepov. Dynamic stiffness analysis of laminated beams using a first order shear deformation theory. *Composite Structures*, 31(4):265–271, 1995. doi: 10.1016/0263-8223(95)00091-7.

[32] P. Vidal, L. Gallimard, and O. Polit. Composite beam finite element based on the proper generalized decomposition. *Computers and Structures*, 102-103(0):76–86, 2012. doi: 10.1016/j.compstruc.2012.03.008.

[33] R.P. Shimpi and Y.M. Ghugal. A new layerwise trigonometric shear deformation theory for two-layered cross-ply beams. *Composites Science and Technology*, 61(9):1271–1283, 2001. doi: 10.1016/S0266-3538(01)00024-0.

[34] E. Onate, A. Eijo, and S. Oller. Simple and accurate two-noded beam element for composite laminated beams using a refined zigzag theory. *Computer Methods in Applied Mechanics and Engineering*, 213-216(0):362–382, 2012. doi: 10.1016/j.cma.2011.11.023.

[35] E. Carrera. Theories and finite elements for multilayered, anisotropic, composite plates and shells. *Archives of Computational Methods in Engineering*, 9(2):87–140, 2002. doi: 10.1007/BF02736649.

[36] E. Carrera. Theories and finite elements for multilayered plates and shells: a unified compact formulation with numerical assessment and benchmarking. *Archives of Computational Methods in Engineering*, 10(3):216–296, 2003. doi: 10.1007/BF02736224.

[37] E. Carrera, G. Giunta, and M. Petrolo. *Beam Structures: Classical and Advanced Theories*. John Wiley & Sons, 2011. doi: 10.1002/9781119978565.

[38] E. Carrera, M. Cinefra, M. Petrolo, and E. Zappino. *Finite Element Analysis of Structures through Unified Formulation*. John Wiley & Sons, 2014.

[39] E. Carrera, G. Giunta, P. Nali, and M. Petrolo. Refined beam elements with arbitrary cross-section geometries. *Computers and Structures*, 88(5–6):283–293, 2010. doi: 10.1016/j.compstruc.2009.11.002.

[40] E. Carrera, M. Cinefra, M. Petrolo, and E. Zappino. Comparisons between 1D (beam) and 2D (plate/shell) finite elements to analyze thin-walled structures. *Aerotecnica Missili e Spazio*, 2014. In Press.

[41] E. Carrera, E. Zappino, and M. Petrolo. Analysis of thin-walled structures with longitudinal and transversal stiffeners. *Journal of Applied Mechanics*, 80, 2013. doi: 10.1115/1.4006939.

[42] E. Carrera, E. Zappino, and M. Filippi. Free vibration analysis of thin-walled cylinders reinforced with longitudinal and transversal stiffeners. *Journal of Vibration and Acoustics*, 135, 2013. doi: 10.1115/1.4007559.

[43] S.M. Ibrahim, E. Carrera, M. Petrolo, and E. Zappino. Buckling of composite thin walled beams by refined theory. *Composite Structures*, 94(2):563–570, 2012. doi: 10.1016/j.compstruct.2011.08.020.

[44] E. Carrera, M. Petrolo, and P. Nali. Unified formulation applied to free vibrations finite element analysis of beams with arbitrary section. *Shock and Vibration*, 18:485–502, 2011. doi: 10.3233/SAV20100528.

[45] A. Pagani, M. Boscolo, J. R. Banerjee, and E. Carrera. Exact dynamic stiffness elements based on one-dimensional higher-order theories for free vibration analysis of solid and thin-walled structures. *Journal of Sound and Vibration*, 332(23):6104–6127, 2013. doi: 10.1016/j.jsv.2013.06.023.

[46] A. Pagani, E. Carrera, M. Boscolo, and J. R. Banerjee. Refined dynamic stiffness elements applied to free vibration analysis of generally laminated composite beams with arbitrary boundary conditions. *Composite Structures*, 110:305—316, 2014. doi: 10.1016/j.compstruct.2013.12.010.

[47] E. Carrera and A. Varello. Dynamic response of thin-walled structures by variable kinematic one-dimensional models. *Journal of Sound and Vibration*, 331(24):5268—5282, 2012. doi: 10.1016/j.jsv.2012.07.006.

[48] M. Petrolo. Flutter analysis of composite lifting surfaces by the 1D Carrera Unified Formulation and the doublet lattice method. *Composite Structures*, 95:539—546, 2013. doi: 10.1016/j.compstruct.2012.06.021.

[49] M. Petrolo. Advanced 1D structural models for flutter analysis of lifting surfaces. *International Journal of Aeronautical and Space Sciences*, 13(2):199—209, 2012. doi: 10.5139/IJASS.2012.13.2.199.

[50] A. Pagani, M. Petrolo, and E. Carrera. Flutter analysis by refined 1D dynamic stiffness elements and doublet lattice method. *Advances in Aircraft and Spacecraft Science*, 1(3):291–310, 2014. doi: 10.12989/aas.2014.1.3.291.

[51] E. Carrera and M. Petrolo. Refined one-dimensional formulations for laminated structure analysis. *AIAA Journal*, 50(1):176–189, 2012. doi: 10.2514/1.J051219.

[52] E. Carrera, M. Filippi, and F. Zappino. Free vibration analysis of laminated beam by polynomial, trigonometric, exponential and zig-zag theories. *Journal of Composite Materials*, 2013. doi: 10.1177/0021998313497775.

[53] E. Carrera, M. Filippi, and F. Zappino. Laminated beam analysis by polynomial, trigonometric, exponential and zig-zag theories. *European Journal of Mechanics A/Solids*, 41:58–69, 2013. doi: 10.1016/j.euromechsol.2013.02.006.

[54] M. Filippi, A. Pagani, M. Petrolo, G. Colonna, and E. Carrera. Static and free vibration analysis of laminated beams by refined theory based on chebyshev polynomials. *Composite Structures*, 132:1248—1259, 2015. doi: 10.1016/j.compstruct.2015.07.014.

[55] M. Carrera, E.and Filippi, P.K.R. Mahato, and A. Pagani. Advanced models for free vibration analysis of laminated beams with compact and thin-walled open/closed sections. *Journal of Composite Materials*, 49(17):2085—2101, 2015. doi: 10.1177/0021998314541570.

[56] G. Giunta, S. Belouettar, and E. Carrera. Analysis of FGM beams by means of classical and advanced theories. *Mechanics of Advanced Materials and Structures*, 17:622—635, 2010. doi: 10.1080/15376494.2010.518930.

[57] D.S. Mashat, E. Carrera, A.M. Zenkour, S.A. Al Khateeb, and M. Filippi. Free vibration of fgm layered beams by various theories and finite elements. *Composites: Part B*, 59:269—278, 2014. doi: 10.1016/j.compositesb.2013.12.008.

[58] G. Giunta, Y. Koutsawa, S. Belouettar, and H. Hu. Static, free vibration and stability analysis of three-dimensional nano-beams by atomistic refined models accounting for surface free energy effect. *International Journal of Solids and Structures*, 50:1460—1472, 2013. doi: 10.1016/j.ijsolstr.2013.01.025.

[59] F. Biscani, G. Giunta, S. Belouettar, E. Carrera, and H. Hu. Variable kinematic beam elements coupled via Arlequin method. *Composite Structures*, 93:697—708, 2011. doi: 10.1016/j.compstruct.2010.08.009.

[60] E. Carrera and A. Pagani. Multi-line enhanced beam model for the analysis of laminated composite structures. *Composites: Part B*, 57:112–119, 2014. doi: 10.1016/j.compositesb.2013.09.046.

[61] E. Carrera and M. Petrolo. On the effectiveness of higher-order terms in refined beam theories. *Journal of Applied Mechanics*, 78, 2011. doi: 10.1115/1.4002207.

[62] E. Carrera, F. Miglioretti, and M. Petrolo. Computations and evaluations of higher-order theories for free vibration analysis of beams. *Journal of Sound and Vibration*, 331:4269—4284, 2012. doi: 10.1016/j.jsv.2012.04.017.

[63] E. Carrera, A. Pagani, and F. Zangallo. Thin-walled beams subjected to load factors and non-structural masses. *International Journal of Mechanical Sciences*, 81:109–119, 2014. doi: 10.1016/j.ijmecsci.2014.02.015.

[64] A. Pagani, F. Zangallo, and E. Carrera. Influence of non-structural localized inertia on free vibration response of thin-walled structures by variable kinematic beam formulations. *Shock and Vibration*, 2014, 2014. Article ID 141982, doi: 10.1155/2014/141982.

[65] E. Carrera and A. Pagani. Accurate response of wing structures to free-vibration, load factors, and non-structural masses. *AIAA Journal*, In Press, 2015. doi: 10.2514/1.J054164.

[66] E. Carrera, M. Filippi, and F. Zappino. Free vibration analysis of rotating composite blades via Carrera Unified Formulation. *Composite Structures*, 106:317–325, 2013. doi: 10.1016/j.compstruct.2013.05.055.

[67] E. Carrera, M. Filippi, and F. Zappino. Analysis of rotor dynamic by one-dimensional variable kinematic theories. *Journal of Engineering for Gas Turbines and Power*, 135(9), 2013. doi: 10.1115/1.4024381.

[68] E. Carrera and M. Filippi. Variable kinematic one-dimensional finite elements for the analysis of rotors made of composite materials. *Journal of Engineering for Gas Turbines and Power*, 136(9), 2014. doi: 10.1115/1.4027192.

[69] A. Varello and E. Carrera. Nonhomogeneous atherosclerotic plaque analysis via enhanced 1D structural models. *Smart Structures and Systems*, 13(4):659–683, 2014. doi: 10.12989/sss.2014.13.4.659.

[70] G. Giunta, D. Crisafulli, S. Belouettar, and E. Carrera. A thermo-mechanical analysis of functionally graded beams via hierarchical modelling. *Composite Structures*, 95:676—690, 2013. doi: 10.1016/j.compstruct.2012.08.013.

[71] F. Miglioretti, E. Carrera, and M. Petrolo. Variable kinematic beam elements for electro-mechanical analysis. *Smart Structures and Systems*, 13(4):517–546, 2014. doi: 10.12989/sss.2014.13.4.517.

[72] E. Carrera, M. Petrolo, and A. Varello. Advanced beam formulations for free vibration analysis of conventional and joined wings. *Journal of Aerospace Engineering*, 24(2):282—293, 2012. doi: 10.1061/(ASCE)AS.1943-5525.0000130.

[73] E. Carrera, M. Petrolo, and E. Zappino. Performance of CUF approach to analyze the structural behavior of slender bodies. *Journal of Structural Engineering*, 138(2):285–297, 2012. doi: 10.1061/(ASCE)ST.1943-541X.0000402.

[74] M. Petrolo, E. Zappino, and E. Carrera. Refined free vibration analysis of one-dimensional structures with compact and bridge-like cross-sections. *Thin-Walled Structures*, 56:49–61, 2012. doi: 10.1016/j.tws.2012.03.011.

[75] E. Carrera, A. Pagani, and M. Petrolo. Classical, refined and component-wise theories for static analysis of reinforced-shell wing structures. *AIAA Journal*, 51(5):1255–1268, 2013. doi: 10.2514/1.J052331.

[76] E. Carrera, A. Pagani, and M. Petrolo. Component-wise method applied to vibration of wing structures. *Journal of Applied Mechanics*, 80(4), 2013. doi:10.1115/1.4007849.

[77] A. Pagani, M. Petrolo, G. Colonna, and E. Carrera. Dynamic response of aerospace structures by means of refined beam theories. *Aerospace Science and Technology*, 46:360—373, 2015. doi:10.1016/j.ast.2015.08.005.

[78] E. Carrera and E. Zappino. Carrera unified formulation for free-vibration analysis of aircraft structures. *AIAA Journal*, In Press, 2015. doi: 10.2514/1.J054265.

[79] E. Carrera, A. Pagani, and M. Petrolo. Refined 1D finite elements for the analysis of secondary, primary and complete civil engineering structures. *Journal of Structural Engineering*, 2014. In Press, doi: 10.1061/(ASCE)ST.1943-541X.0001076.

[80] E. Carrera and A. Pagani. Free vibration analysis of civil engineering structures by component-wise models. *Journal of Sound and Vibration*, 2014. In Press, doi: 10.1016/j.jsv.2014.04.063.

[81] E. Carrera, M. Maiarú, and M. Petrolo. Component-wise analysis of laminated anisotropic composites. *International Journal of Solids and Structures*, 49:1839–1851, 2012. doi: 10.1016/j.ijsolstr.2012.03.025.

[82] E. Carrera, M. Maiarú, M. Petrolo, and G. Giunta. A refined 1D element for the structural analysis of single and multiple fiber/matrix cells. *Composite Structures*, 96:455—468, 2013. doi: 10.1016/j.compstruct.2012.09.012.

[83] M. Petrolo, E. Carrera, and A.S.A.S. Alawami. Free vibration analysis of damaged beams via refined models. *Advances in Aricraft and Spacecraft Sciences*, In Press, 2015. In Press.

[84] J.N. Reddy. *Mechanics of laminated composite plates and shells. Theory and Analysis*. CRC Press, 2^{nd} edition, 2004.